Barrier Height Reduction to 0.15eV and Contact Resistivity Reduction to 9.1×10^{-9} Ω-cm^2 Using Ultrathin TiO_{2-x} Interlayer between Metal and Silicon

A. Agrawal[1], J. Lin[1], B. Zheng[2], S. Sharma[2], S. Chopra[2], K. Wang[1], A. Gelatos[2], S. Mohney[1]and S. Datta[1]
[1]The Pennsylvania State University, University Park, PA 16802, USA; [2]Applied Materials, Santa Clara, CA, USA
Email: ashish@psu.edu

Abstract: Metal-insulator-Si (MIS) tunnel contact is studied using ultrathin, non-stoichiometric TiO_{2-x} interlayer on n- and n+ Si. Systematic analysis indicates a record low Schottky barrier height (SBH) of 0.15eV for Ti metal using 10A thick TiO_{2-x} interlayer (T_{Ins}). Ti/TiO_{2-x}/n+ Si contact achieves a record low specific contact resistivity (ρ_c) of $9.1\times10^{-9}\Omega$-cm^2.The modeling of ρ_c suggests tunneling mass, m^*_{Tunnel}, of $0.7m_0$ for TiO_{2-x} compared to stoichiometric TiO_2 indicating transition from an insulator to a wide gap semiconductor.

Introduction: The ON-state channel resistance in nMOSFETs has continually reduced with geometrical scaling and strain engineering, resulting in the external resistance, R_{ext}, is as the dominant component limiting nMOS performance. The main contributor to R_{ext} is the interface resistance, R_{CO}, between the S/D region and the metal silicide layer. Materials screening shows that most, if not all, metals suffer from strong Fermi level pinning close to the mid-gap of Si resulting in ~0.65eV barrier height to conduction band. In this work, we investigate lowering of R_{CO} by inserting an ultra-thin dielectric, TiO_2, exhibiting low conduction band offset (CBO) and low m^*_{Tunnel} between the metal and semiconductor interface (Fig. 1, 2).

Device Fabrication and Characterization: We fabricated Schottky diodes on n$^-$ doped Si ($N_D=10^{15}$/cm^3) to extract Schottky barrier height, SBH, and fabricated Refined Transmission Line Method (RTLM) structures [1] on n$^+$ doped Si ($N_D=1.4\times10^{20}$, 3×10^{20} and 4.1×10^{20}/cm^3) to extract ρ_c. After surface pre-clean step,an ultra-thin TiO_2 dielectric was deposited using atomic layer deposition (ALD) for MIS contact followed by metal patterning using standard lithography and lift-off. Fig. 3(a,c) shows the cross sectional transmission electron microscopy (TEM) image of the MIS contact with T_{Ins} of ~1nm. Fig. 3(b) shows XPS spectra of Ti and O prior to metal deposition, showing Ti^{4+} and O^{2-} peaks indicating stoichiometric TiO_2 with O/Ti=2.1/1. Electron energy loss spectrum (EELS) (Fig. 3(d)) analysis of the MIS contact shows a strong Ti signal and a weak O signal at the interface indicating oxygen deficient, non-stoichiometric TiO_{2-x} interlayer at the interface due to oxygen gettering by the overlying Ti metal.

SBH Tuning: Increasing the T_{Ins} reduces the metal induced gap states, MIGS occupancy, thereby unpinning the metal Fermi level from the Si charge neutrality level (CNL) [2]. The metal Fermi level aligns with the TiO_2 CNL which is close to the Si conduction band edge (Fig. 4). Fig. 5(a) shows the measured J-V characteristics for Ni/n- Si and Ni/TiO_{2-x}/n- Si MIS contact with T_{Ins}=10A and 20A. MIS contact exhibits 300X higher reverse saturation current for T_{Ins}=20A than the pinned Ni/n- Si. SBH extracted using I-V-T measurements (Fig. 5(b)) indicate 3X and 5X reduction for 10A and 20A T_{Ins}, respectively compared to M-S contact.

M-I-S Pinning Factor Extraction: To systematically explore unpinning of Fermi level with respect to Si, Ti, Mo, Ni and Pt metals spanning a workfunction range of ~1eV were deposited on n-Si for SBH extraction on control and MIS contact structure with 10A T_{Ins}. Fig. 6(a,b) show the J-V results showing significantly higher current densities with MIS contact compared to M-S contact. Fig. 7(a,b) shows the Richardson plot of ln(J/T^2) vs. 1000/T for the four deposited metals on control and MIS contact with 10A T_{Ins}. SBH is extracted from the slope of the Richardson plot and is plotted as a function of metal workfunction in Fig. 8. The pinning factor, S which determines the strength of Fermi level pinning at the CNL is extracted from the slope of SBH vs. metal workfunction. Low S factor of 0.075 is extracted for M-S contact confirming pinned Fermi level near midgap for silicon. For MIS contact with 10A T_{Ins}, 3.2× higher S factor of 0.24 is extracted with barrier height approaching near silicon conduction band-edge and SBH reduced to 0.15eV for low workfunction metal, Ti. This indicates that low resistivity MIS contact can be achieved with ultra-thin TiO_{2-x} interlayer and low workfunction metal, Ti, on heavily doped Si.

Contact Resistivity: Contact resistivity is extracted using RTLM structure (Fig. 9(a)) with sub-micron gap spacing for control and MIS contact on heavily doped Si with Ni and Ti metals. The Si active doping was determined from Hall measurement (Fig. 9(b)). Fig. 10 shows the measured J-V characteristics on RTLM indicating 6× increase in current density for 10A T_{Ins}. Specific contact resistivity values, extracted for both Ni and Ti vs. TiO_{2-x} T_{Ins} (Fig. 11,12), show reduction in ρ_c indicating Fermi level unpinning. ρ_c for Ti/(10A)TiO_{2-x}/n+Si is as low as $9.1\text{x}10^{-9}\Omega$-cm^2, achieving 94% reduction compared to the control Ti/n+Si case. For thicker TiO_{2-x}, the tunneling resistance of the interlayer dominates, increasing overall ρ_c as observed for 20A T_{Ins}. We investigate the effect of semiconductor doping on ρ_c for control and MIS contact (Fig. 13). A 3X reduction in ρ_c was obtained for MIS contact 10A T_{Ins} over Si doping range studied.

M-I-S Contact Reliability: Thermal annealing in N_2 ambient was performed to test thermal stability of these contacts (Fig. 14). ρ_c for MIS contact remained unchanged whereas 40% reduction in MS ρ_c was observed at 400C. At 500C, Ti diffusion through RTLM gap spacing was observed. Voltage ramp-up stress with varying RTLM gap spacing show the electric field-driven breakdown of the MIS contact (Fig. 15(a)), with the breakdown voltage drop of 0.9V at the contact (Fig. 15(b)).

Conclusion: Fig. 16 shows the experimental and modeled ρ_c vs. T_{Ins} for Ti/TiO_{2-x}/n+Si with Φ_{Bn}=0.15eV. The TiO_{2-x} shows 4.3X reduced $m^*_{Tunnel}=0.7m_0$ vs. $3m_o$ in stoichiometric TiO_2 [3][4] indicating transition from insulator to wide bandgap semiconductor. Table I benchmarks the SBH and ρ_c for various MIS contacts on n- Si till date. Here, we demonstrate the lowest SBH of 0.15eV and the lowest ρ_c of $9.1\text{x}10^{-9}\Omega$-cm^2 on n+Si using 10A thick non-stoichiometric TiO_{2-x} interlayer owing to significantly reduced m^*_{Tunnel}.

References

[1] R. Dormaier et.al., *JVAC*, 2012 [5] B. Coss et.al, *VLSI*, 2009
[2] A. Agrawal et.al. *APL*, 2012 [6] K. Ang et.al., *IEDM*, 2012
[3] G. Dewey et. al. U.S. Patent Application # 0327377, 2010
[4] J. Pascaul et.al., *PRL*, 1977

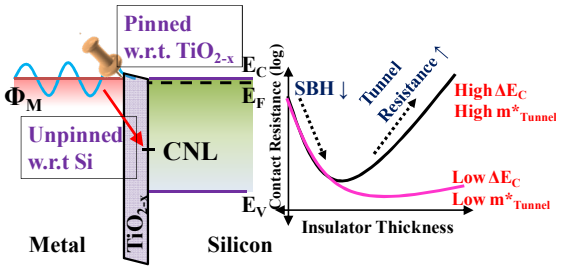

Fig. 1(a): Schematic of metal-TiO_{2-x}-Si showing Fermi level unpinning and reduction in effective barrier height; (b) Both low ΔE_C and m^*_{Tunnel} required to achieve low ρ_C.

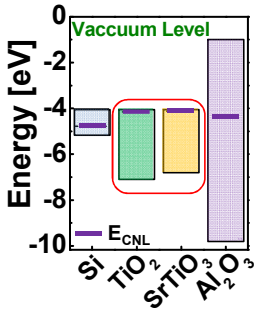

Fig. 2: Low conduction band offset between TiO_2 and Si makes it ideal candidate as interlayer.

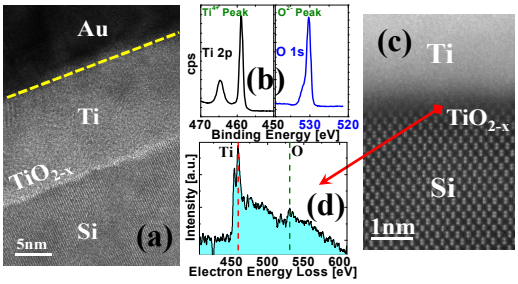

Fig. 3(a): TEM of MIS contact with TiO_{2-x} interlayer; (b) XPS spectra (before Ti deposition); (c) Dark field STEM of Ti/TiO_{2-x}/Si MIS contact; (d) EELS spectrum showing Ti and weak O signal indicating non-stoichiometric, oxygen-deficient interlayer after Ti deposition

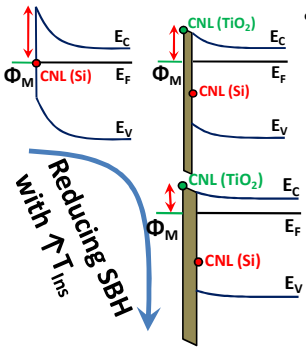

Fig. 4: Schematic showing unpinning and FL movement towards insulator CNL

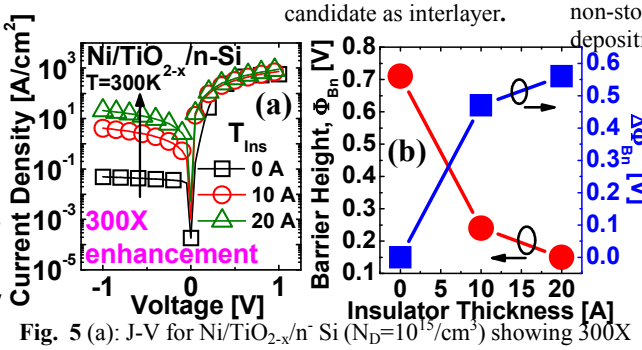

Fig. 5 (a): J-V for Ni/TiO_{2-x}/n^- Si (N_D=10^{15}/cm^3) showing 300X enhancement compared to Ni/n^-Si; (b) Extracted Φ_{Bn} as a function of insulator thickness from I-V-T measurement show 3X reduction for 10A and 5X for 20A T_{Ins}

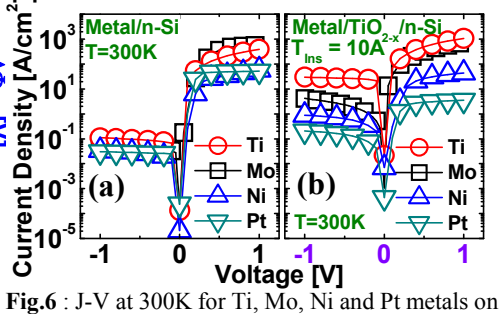

Fig.6 : J-V at 300K for Ti, Mo, Ni and Pt metals on (a) n^- Si for MS; (b) (10A)TiO_{2-x}/n^- Si MIS contact

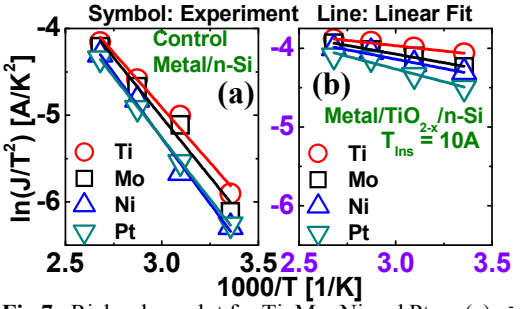

Fig.7 : Richardson plot for Ti, Mo, Ni and Pt on (a) n^- Si MS contact; (b) (10A)TiO_{2-x}/n^- Si MIS contact

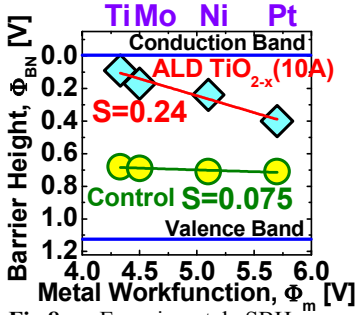

Fig.8 : Experimental SBH vs. workfunction for metal/n^- Si and metal/TiO_{2-x}/n^- Si.

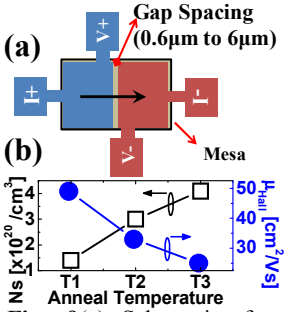

Fig. 9(a): Schematic of RTLM structure;(b) Substrate doping and hall mobility as a function of anneal

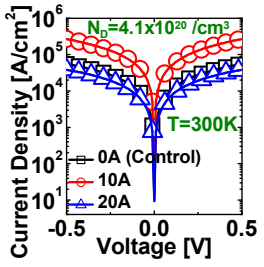

Fig. 10: J-V for Ti/n^+ Si and Ti/TiO_{2-x}/n^+ Si for varying T_{Ins}, showing significant current enhancement for MIS contact

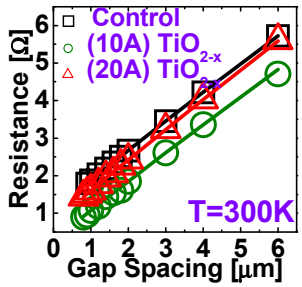

Fig. 11: RTLM resistance vs. gap spacing for MS and MIS contact with T_{Ins}=10A and 20A

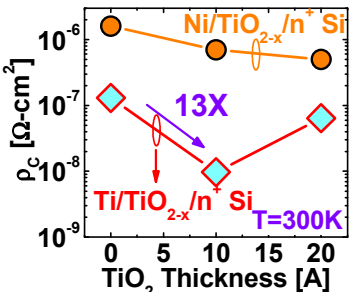

Fig. 12: Extracted ρ_C vs. T_{Ins} with Ti and Ni metals. 13X reduction was observed with Ti metal and 10A T_{Ins}

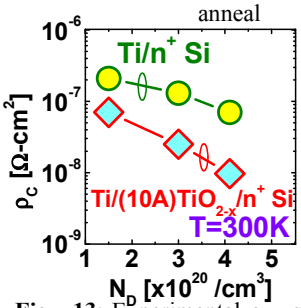

Fig. 13: Experimental ρ_C vs. Si substrate doping density, N_D for MS and MIS contacts

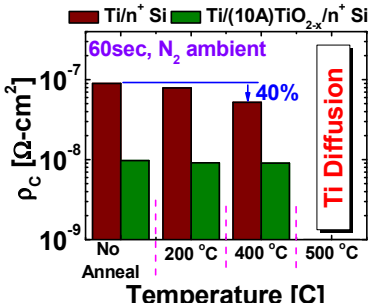

Fig. 14: Experimental ρ_C for MS and MIS contact for different annealing temperatures in N_2 ambient

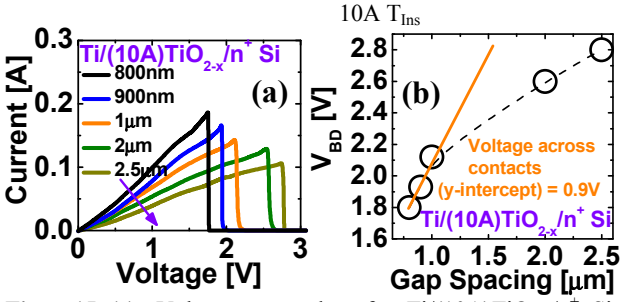

Fig. 15 (a): Voltage stress data for Ti/(10A)TiO_{2-x}/n^+ Si contact; (b) Breakdown voltage vs. TLM gap spacing.

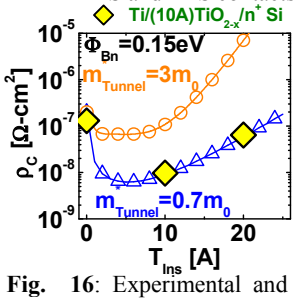

Fig. 16: Experimental and modeled ρ_C vs. T_{Ins} for Ti/(10A)TiO_{2-x}/n^+ Si

Reference	Metal	Interlayer	Doping [/cm^3]	Barrier Height [eV]	Contact Resistivity [Ω-cm^2]
Coss et. al. [5]	TaN	La_2O_3/SiO_2	10^{18}	0.12	--
Ang et. al. [6]	--	La_2O_3	$3x10^{20}$	--	$9.5x10^{-9}$
Ang et. al. [6]	--	La_2O_3/SiO_2	$3x10^{20}$	--	$1.25x10^{-7}$
This Work	Ti	TiO_{2-x}	$4.1x10^{20}$	0.15	$9.1x10^{-9}$
This Work	Ti	TiO_{2-x}	$3x10^{20}$	0.15	$2.4x10^{-8}$

Table I: Benchmarking SBH and ρ_C of various MIS contact schemes on n-doped Si substrate